Coupling of solvent-free synthesis and reactive extrusion of alumina: an ecologically efficient integration for heterogenous catalyst synthesis

Pierre-Igor Dassie, Ryma Haddad, Maud Lenez, Alexandra Chaumonnot, Malika Boualleg, Patrick Legriel, Ales Styskalik, Bernard Haye, Mohamed Selmane, Damien Debecker, et al.

Coupling of solvent-free synthesis and reactive extrusion of alumina: an ecologically efficient integration for heterogenous catalyst synthesis†

Pierre-Igor Dassie,‡[a] Ryma Haddad,[a] Maud Lenez,[a] Alexandra Chaumonnot,[b] Malika Boualleg,[b] Patrick Legriel,[a] Ales Styskalik,[d] Bernard Haye,[a] Mohamed Selmane,[c] Damien P. Debecker,[d] Clement Sanchez,[a] Corinne Chaneac[a] and Cedric Boissiere*[a]

Innovation in materials manufacturing processes is a challenge to reduce the environmental impact of the chemical industry in line with sustainable development objectives, such as promoting sustainable industrialization and ensuring responsible consumption and production patterns. One of the ways to reach this goal is to revisit the main synthesis processes and to rethink their use. Reactive extrusion is a well-known continuous process used to produce and shape various materials in the polymer and food industries, but hardly leads to the direct synthesis and shaping of metal oxide materials (ceramics). In contrast, sol–gel chemistry offers tremendous opportunities to synthesize metal oxide networks by polycondensation of molecular precursors at a low temperature, but it is mostly operated in sluggish batch processes, using massive amounts of solvent contaminants and producing large amounts of chemical waste (*E*-factor > 40). In this work, for the first time, we coupled extrusion with sol–gel chemistry to produce high surface area shaped alumina-based materials that meet or exceed the requirements to be used as heterogeneous catalysts or catalyst supports. The necessity to adapt sol–gel chemistry – usually done in a diluted environment – to meet the twin-extruder technical constraints – usually working in a viscous environment – led to a peculiar choice of reaction conditions little discussed in the literature: the hydrolysis/condensation of (solid) alkoxide precursors without a solvent. We were able to synthesize and shaped high specific surface area boehmite (γ-AlOOH) at room temperature, in a continuous mode, and under solvent-free conditions. The solids are directly shaped in the form of self-standing "spaghetti" or extrudates. Upon calcination, the shaped hydroxides are converted into mesoporous and high specific surface area gamma alumina (γ-Al_2O_3) materials. We show that such materials exhibit high catalytic activity in the dehydration of ethanol. The process intensification presented here paves the way towards very low-waste, low-energy, and – all in all – more sustainable manufacturing practices for shaped high surface area metal oxides. In addition, it could be potentially less expensive since the simplification of the equipment and the lower energy consumption will contribute to drastically reduce the production costs even if the

Introduction

Catalysts are an essential cornerstone of industrial chemistry, especially for sustainable chemical process development since they allow massive production of chemical commodities at a lower cost. They are used in many fields: energy,[1,2] environment[3–5] and materials.[2,6]

Heterogeneous catalysts are favored whenever possible for they allow performing the same reaction multiple times, with lower energy input, and, in some cases, they can be operated in a continuous flow mode for a long time on stream.[7–9] Their structure and composition can be complex according to the

targeted reaction. They are usually made of an active phase dispersed onto a mechanically and chemically robust porous support. The shape of the support is adapted to the type of the reactor; it can be powders, extrudates, monoliths, *etc.*[9–13]

While efficient heterogeneous catalysts are essential to develop effective and sustainable chemical processes, the environmental and economic burden of their preparation itself must also be considered in the evaluation of any proposed catalytic technology.[14] The preparation of catalysts and catalyst supports usually requires multi-step syntheses to control textural and mechanical properties that generate large amounts of (liquid and gaseous) wastes and are often energy intensive. Gamma alumina (γ-Al_2O_3) is one of the more representative support catalysts from the family of transition alumina that can be produced efficiently and reproducibly, with controlled size and shape, by topotactic dehydration of γ-AlOOH (boehmite). γ-Al_2O_3 is commonly used as a catalyst support at the industrial scale for oil refinery, especially for reforming,[15,16] hydro-treatment[17] and hydro-conversion[18] reactions and also for alcohol dehydration to alkenes and in the Claus process.[19,20] γ-Al_2O_3's interest resides in its highly modular textural properties, which can be tuned by the size and morphology of primary boehmite particles, their shaping process (peptization and neutralization steps), and its quite low reactivity coupled with a good mechanical strength.[21–23]

The preparation of ready-to-use alumina-based catalysts is a long and quite expensive process including at first several steps for boehmite nanoparticle synthesis and then a shaping process as shown Fig. 1.[24,25] The conventional synthesis protocols for boehmite imply a multi-step approach depending on the synthesis strategy. The sol–gel method, also known as the Yoldas process, uses metal alkoxides as precursors with an excess of water (H_2O/Al is around 200/1).[26] In industry, the most common strategy is the neutralization of an aqueous acidic solution of metal salt precursors (such as $Al(NO_3)_3$,[27–29] Al_2SO_4,[29–31] or $AlCl_3$[32]) by a basic solution of aluminate,[33] NaOH,[28] ammonia[29] or urea.[29,31] The as-obtained precipitate corresponding to boehmite is usually aged in the mother liquor at atmospheric or higher pressure at different temperatures (from room temperature to 150 °C).[28,34] Afterward, the solid is filtered from the reaction medium, and washed several times with a large amount of water, at room temperature or higher, to eliminate the counter-ions from the aluminum salts. Then the wet powder, named "filtration cake", is dried in an oven. Apart from precisely controlling the texture, crystalline structure, and surface properties of alumina powders, catalysis scientists must also consider the shaping of the latter into larger catalyst bodies (microsphere, extrudates, monolith, *etc.*) that can be handled easily and loaded in flow reactors without causing excessive pressure-drop.[35–38] This kneading–extrusion process includes the peptization of the powder in a liquid, usually an acid or base, and potentially with an organic or mineral additive before extrusion. Peptization leads to deagglomeration of particles due to electrostatic repulsion of the

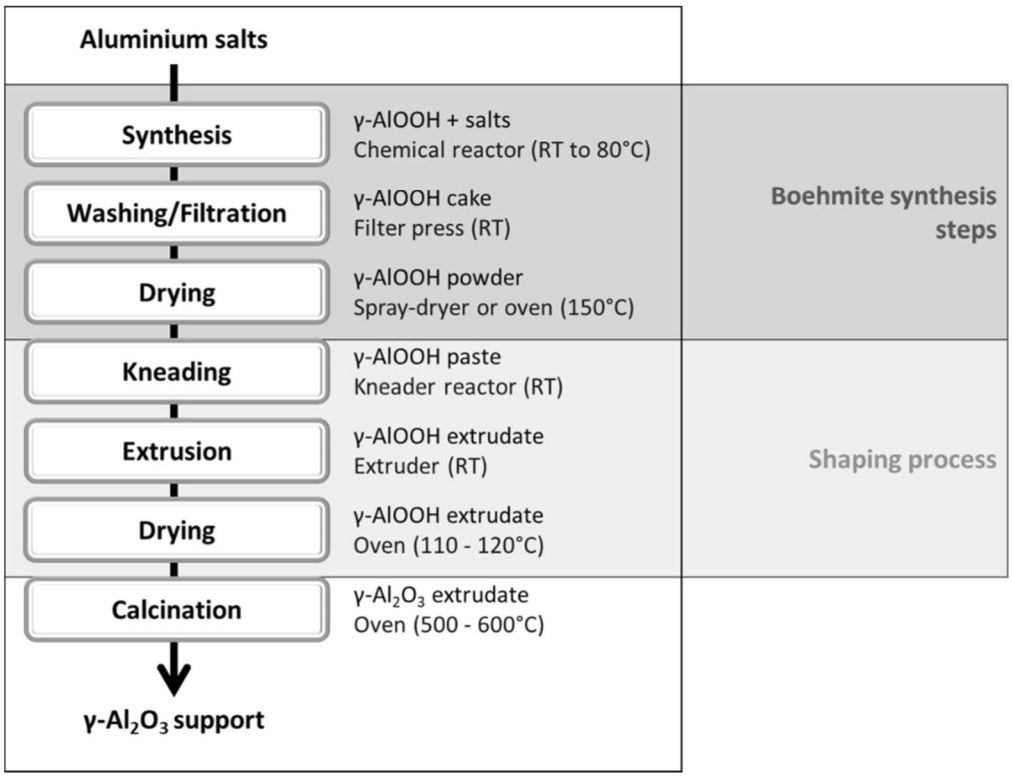

Fig. 1 Schematic view of a conventional multi-step[21,34] production route for γ-Al_2O_3 catalyst supports from aluminum salts in the industry. RT stands for room temperature.

charged surface after the adsorption of protons or hydroxyl ions. Finally, in order to transform boehmite into γ-Al_2O_3, a calcination step is performed, usually between 500 and 700 °C.[39,40] The final textural properties of the support are mainly set during boehmite synthesis, but it can be modulated to a certain degree during the shaping process.[35]

As shown in Fig. 1, before calcination, at least six elementary steps are necessary to obtain γ-Al_2O_3 shaped extrudates *via* the conventional precipitation methods. Each step requires a different device, different temperature and different completion time. In most cases, each step is carried out in a batch mode. One of the many consequences of this processing pathway is that a very large volume of the solvent (mostly water) is used. Also, binding agents[41] and porogens can be added in order to improve extrudate cohesion before thermal treatment and to achieve the required textural properties, respectively. Based on rare published reports,[42,43] the production of γ-Al_2O_3 extrudates produces a lot of liquid waste. In the literature, the weight of effluents generated by the washing of aluminum counter ions is rarely quantified (from our experience, several times the same amount of, sometimes hot, water used for precipitation). Furthermore, the overall production process is discontinuous. This conventional approach is highly unsatisfactory from a sustainability point of view: poor atom economy, large waste production (high *E*-factor), and high energy consumption.

A possible way to tackle this problem is to regroup as many steps as possible into one single device, using a drastic economy of atoms and energy. With this later considerations, reactive extrusion is an interesting process to develop for the intensive production of such catalysts. First, the extrusion process is a shaping process, well known in the industry and widely used to shape metal oxide catalysts or catalyst supports such as γ-Al_2O_3. The reactive extrusion process is about using a continuous extruder as a chemical reactor and a shaping tool. Indeed, a chemical reactor with a large contact surface area is able to transfer heat to/from the reactive medium. The modularity of its screw profile allows performing the transport, mixing, and shearing of matter, and it can accommodate highly viscous media. Reactive extrusion has been used for a long time for organic polymerization or polymer modifications[44,45] in the industrial field.[45] Its recent development is focused on hybrid materials.[44,46] Despite its obvious potential for the synthesis and shaping of metal oxide materials, like γ-AlOOH boehmite, no information has been published on the subject to our knowledge.

In this paper, the production of shaped gamma alumina is revisited by combining the extrusion process with sol–gel chemistry,[47] which is known for its ability to produce metal oxides under mild experimental conditions and its adaptability to industrial processing. Intrinsically, aluminum-based sol–gel reactions require large amounts of heated solvents to control hydrolysis and condensation steps, and lead to boehmite particles of controlled shape and size which are crucial for obtaining highly porous active and selective catalysts.[26,48–51] In the literature, the precipitation of boehmite from aluminum alkoxide precursors also uses large amounts of solvents for controlling the high reactivity and exothermicity of the hydrolysis step.[26] In contrast, a few recent scholarly publications[40,52–58] mention the facile synthesis of boehmite at ambient temperature by using a solvent-free synthesis in which aluminum alkoxides and a very small amount of water, used as a reactant, are ground using a hand mortar. These reports focused on the final characteristics of the γ-Al_2O_3 particles obtained after calcination but no investigation was presented on the properties of the boehmite intermediates or on the influence of processing parameters. More specifically, the high exothermicity of the alkoxide hydrolysis reaction was not discussed, even though it is likely to strongly influence the final product characteristics for the reaction temperature depends on the amount of matter reacted at a time. Looking for a strategy allowing eliminating liquid waste completely, we concluded that the direct use of alkoxide precursors in a solvent-free reaction can be an efficient synthesis approach.

Here, we disclose for the first time a solvent-free, binder-free, and porogen-free synthesis and shaping strategy of high surface area mesoporous γ-AlOOH extrudates using a near ambient temperature, one-step-one-tool process of reactive extrusion. After calcination, γ-AlOOH extrudates lead to γ-Al_2O_3 with a high specific surface area and porous volume. As a reference, extrudates are also prepared from boehmite particles obtained under the same chemical conditions but using a batch process followed by the usual kneading–extrusion process (including peptization/neutralization steps). The obtained γ-Al_2O_3 extrudates were tested for the alcohol dehydration reaction and compared to a commercial alumina powder.

Materials and methods

Chemicals

The following chemicals were used: aluminum tri-*sec*-butoxide (ASB) 97% from Sigma-Aldrich and aluminum isopropoxide (AIP) 98% from Sigma-Aldrich. Milli-Q water was used for alkoxide hydrolysis. AIP was ground with a mortar before use (the ground powder was analyzed before use by FTIR spectroscopy to ensure that it wasn't hydrolyzed/condensed during grinding or storage). Commercial boehmite (Pural SB3) obtained from Sigma-Aldrich was used as a reference for characterization.

Reactive extrusion of γ-AlOOH mesoporous extrudates

Scamex's Twin Screws Micro-Extruder (TSME) of 60 cm length with 18 mm diameter screws was used. The temperature of the device was set at 30 °C (corresponds to room temperature during summer time) and the screw speed was set at 300 rpm. The screw profile of the mixing area (Fig. SI.1 B†) was selected by comparing the kneading, transport, and mixing moduli in terms of the textural properties of the materials produced at various temperatures and hydrolysis rates (experiments not presented here). We selected the kneading profile that gave boehmite with a highly reproducible surface area and porous

volume and that was reasonably stable with hydrolysis rate variations and the aluminum alkoxide source. Water was fed through the hopper (H2 in Fig. SI.1 A†) using a peristaltic pump at 1.32 and 1.76 ml min^{-1} (corresponding to a water/aluminum molar hydrolysis ratio "*h*" of 6 and 8, respectively). AIP was fed using a doser through the next hopper (H3 in Fig. SI.1 A†), which is closest to the head extruder at a constant feed of 2.5 g min^{-1}. The feeding rate of aluminum alkoxide and water was chosen for producing as much boehmite as possible, while maintaining a constant water/alkoxide molar ratio. We determined the limit by increasing the doser feeding rate until the feeding hopper was blocked. Feeding rates provided in the manuscript are about 20% below the limit of our device. The mixing/shearing of AIP and water takes place between the third hopper and the die. It corresponds to a length of 18 cm along the screws, which includes three functional segments: one for transport, one for kneading and one for transport/compression (Fig. SI.1 B†). Samples are collected fifteen minutes after a solid comes out from the extruder corresponding to the stabilization time. We checked that the production rate is constant without changing the appearance of the as-obtained material.

The reaction medium minimum residence time (MRT) was measured by adding a dye, rhodamine B, with AIP through the third hopper H3. The MRT is the time between the dye addition and color appearance of the extruded reaction medium. For our samples the MRT remained stable at 46–48 seconds.

Mechanically-mixed solvent-free synthesis of γ-AlO(OH) mesoporous powders (batch)

Powder samples were prepared by mechanical mixing with an anchor in a polypropylene bottle for 10 minutes at 900 rpm at room temperature, 0.5 mol of precursors (123.2 g of ASB or 102.1 g of AIP) with 3 mol of water for ASB ($h = 6$) and 2.5 mol of water for AIP ($h = 5$), respectively. The cake was dried under vacuum for 14 hours at room temperature. Around 30 g of powder was produced for each precursor.

γ-AlOOH mesoporous powder shaping into extrudates by kneading and extrusion

The powder of each precursor obtained from a mechanically mixed solvent-free synthesis was kneaded and subjected to a peptization (addition of an acid solution, HNO_3)/neutralization (addition of a basic solution, NH_4OH) process to minimize aggregation defects and achieve an adequate viscosity to allow shaping by extrusion. The kneading of boehmite powder was performed with a standard kneader aside from the extrusion device. In a typical experiment, 31 g of dry boehmite powder was introduced into a kneader. Then, 20 mL of nitric acid solution was added to achieve a HNO_3/Al molar ratio of 5%. After 105 min of kneading, 0.8 mL of NH_4OH solution (3.73 M) and 3.3 mL of water were added in order achieve a NH_4OH/HNO_3 molar ratio of 20%. Extrusion was performed with a press extruder and a trilobe shape with a pressure in the 100–150 bar range.

Extrudates samples prepared this way are labeled as follows: *Processing_Precursor_hydrolysis ratio_ post processing.* Processing can be either kneading–extrusion (KE) or reactive extrusion (RE). For post-processing, fresh materials, dried materials and calcined materials are labeled (F), (D) and (C) respectively. For example, fresh extrudates prepared from IPA with a hydrolysis ratio of 6 by reactive extrusion is labeled "RE_IPA_6_F", while a calcined extrudate made from an already prepared boehmite obtained with ASB using a hydrolysis ratio of 5 and shaped in a second time by kneading followed by extrusion is labeled "KE_ASB_5_C".

Characterization techniques

Fourier-transform infrared (FTIR) spectroscopy was carried out using a Spectrum 400 FT-IR/FT-NIR de PerkinElmer© spectrometer. Attenuated total reflectance (ATR) measurements were performed as follow: samples were scanned 16 times from 550 to 4000 cm^{-1} with a resolution of 1 cm^{-1} at room temperature. Transmittance measurements were performed with a KBr binder. The analysis procedure was 16 scans from 400 to 4000 cm^{-1} with a resolution of 1 cm^{-1} at room temperature.

X-Ray diffraction (XRD) was carried out using a low angle Bragg–Brentano Bruker D8 ADVANCE diffractometer using filtered Cu Kα radiation over a 2θ range from 4° to 80° with a step size of 0.02°. To calculate an apparent size of the particles in all the *hkl* dimensions, the Scherrer equation was used.

Scanning electron microscopy (SEM) was carried out using a Hitachi S-3400N.

Transmission electron microscopy (TEM) was carried out using a TECNAI 120 Spirit Twin at an acceleration voltage of 120.0 kV with a Gatan Orius 1000 camera model.

Nitrogen physisorption measurements were carried out using a BELSORP-max de MicrotracBEL©. Before the measurement, the samples were degassed under a primary vacuum, (110 °C for 6 hours for boehmite and 250 °C for 3 hours for gamma alumina) to remove any adsorbed organic compounds and water. The Brunauer–Emmett–Teller (BET) method was used to determine the specific surface area and the BJH model was used for the determination of pore size distributions.

The measurement of the crushing strength was carried out with a servo-hydraulic testing system Instron 8502 (High Wycombe, UK) associated with a 5000 N load cell.

Ethanol dehydration

Catalytic tests were performed as described by A. Styskalik *et al.* 2020.[59] The tests were carried out at atmospheric pressure, WHSV = 1.1 h^{-1}. The analysis temperature was varied stepwise (210, 255 and 315 °C). One step consisted of (i) the heating ramp (5 °C min^{-1}) and stabilization at the set temperature (21 min) and (ii) the steady temperature state (63 min). The catalysts were diluted with glass beads (0.5–1 mm) in order to maintain the volume of the catalyst bed constant and silica beads were added to fill the void of the reactor. Catalytic tests were performed with absolute ethanol, which is injected at a 0.212 g h^{-1} rate using a NE-300 syringe pump in a 40 cm^3 min^{-1} flow of N_2 (4.4 mol% of ethanol in N_2). The effluent gas

was analyzed using a VARIAN 3800 gas chromatograph (9 injections at each temperature) equipped with a flame ionization detector (FID) and a Cydex B column (25 m long, internal diameter 0.22 mm, and film thickness 0.25 μm).

Results and discussion

So far, the one-step manufacturing of mesoporous γ-AlOOH extrudates remains essentially unexplored and was never reported. Industrially and in the literature, the synthesis and shaping of γ-AlOOH particles are carried out in separate steps. The final extrusion processing often requires a peptization/neutralization step performed by kneading to increase the adhesive forces between compressed granules that form an extrudate. It removes the macroporosity coming from boehmite aggregates and ensures the mechanical strength of the final product before calcination.[41] In one-step manufacturing of mesoporous γ-AlOOH extrudates without peptization, extrudates would hold together only by van der Waals forces and hydrogen bonds, reducing considerably their ability to maintain shape and their mechanical strength after extrusion. Still, to go further with atom economy, we searched for a strategy to avoid the use of any binder. To safeguard the mechanical integrity and cohesion between elementary boehmite crystals, we inferred that it would be more coherent to form them as much as possible after extrusion (in this way, the shear stress inside the device is not likely to break inter-crystal chemical bonds). Thus, the reactive medium (alumina precursor and water) was extruded and pre-formed before the sol–gel condensation reaction was completed. In addition, this allows to control the residence time of the material in the device.

Following this train of thoughts, in order to reduce the observed reaction kinetics, chemical and processing parameters were adjusted in a way that allowed controlling the diffusion rates and minimizing the reaction medium residence time in the extruder: AIP was chosen as the sol–gel precursor. Theoretically, AIP, which is a solid, is more reactive than ASB, which is a liquid, but in a solvent-free reaction, AIP hydrolysis/condensation takes more time than ASB due to its solid state (water diffusion into aluminum precursor's grains is much slower).

In this manuscript, we report reactive extrusions performed with two hydrolysis ratios (h = 6 and h = 8). Extrusion was not managed below a hydrolysis ratio of 6 due to extruder stuffing, and it was not performed above a hydrolysis ratio of 8 to avoid bayerite phase (α-Al(OH)$_3$) formation as a co-product of boehmite, as it was observed by Huang *et al.*[54] Fresh extrudates obtained for a hydrolysis ratio of 6 and 8 are named RE_AIP_6_F and RE_AIP_8_F, respectively.

To verify that reaction medium extrusion is performed before the complete hydrolysis of AIP, the freshly extruded product was analyzed by FTIR spectroscopy. The infrared spectra of the AIP sol–gel precursor, and freshly extruded RE_AIP_6_F and RE_AIP_8_F are shown in Fig. 2.

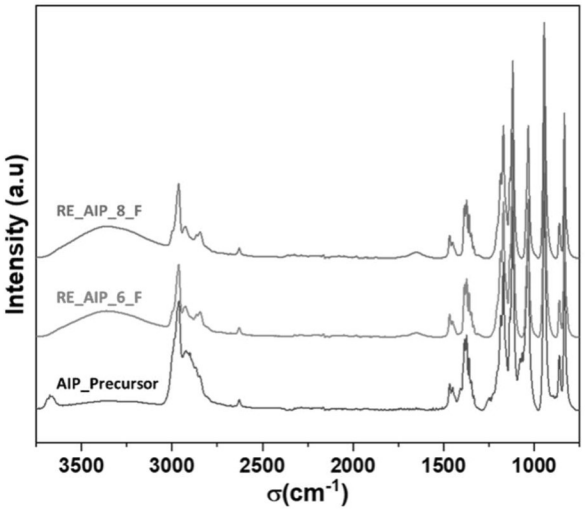

Fig. 2 Infrared spectra of the AIP sol–gel precursor in black, RE_AIP_6_ F (freshly extruded with h = 6) in red and RE_AIP_8_F (freshly extruded with h = 8) in blue.

Similar bands are observed in all three compounds. Most bands are associated with the isopropyl group: the C–H stretching mode of the CH_3 and CH groups is between 2975 and 2850 cm^{-1},[60] C–H bending and rocking modes between 1465 and 1340 cm^{-1} and the C–CH_3 stretching mode[61] with a single band at around 950 cm^{-1}. The C–O stretching mode is observed between 1100 and 1170 cm^{-1}. The bands at 860, 700, 674, 610 and 570 cm^{-1},[62,63] are assigned to tetrahedral and octahedral Al–O vibrations.[64] The (Al)–O–C peak, characteristic of the μ2-bonds of alkoxide, is visible at 1033 cm^{-1},[65] and is found in both extruded compounds, confirming that AIP hydrolysis is still in progress after extrusion. Finally, two peaks absent for the AIP precursor, appear for RE_AIP_6_ F and RE_AIP_8_F: a large and intense band at around 3330 cm^{-1} assigned to the water and alcohol O–H stretching mode, and a small band at 1645 cm^{-1} assigned to the water bending mode. Their appearance is expected since water is added to AIP as a reagent, and AIP hydrolysis generates isopropanol.

Study of hydrolysis kinetic

The RE_AIP_8_F sample was analyzed by ATR FTIR spectroscopy after aging at room temperature for different time intervals (60, 90, 105 and 120 minutes). Infrared spectra of the RE_AIP_8_F sample are shown in Fig. 3. By comparing the sample at 0 and 60 minutes after extrusion, the C–H stretching modes at 2975 and 2850 cm^{-1} decrease fast if compared with the large band related to water, and Al–OH and alcohol O–H stretchings at around 3000–3500 cm^{-1} (the later decreases slowly with the progressive evaporation of alcohol). Bands of the O–H bending mode at 1300 cm^{-1} and C–O symmetric stretch at 815 cm^{-1} corresponding to a characteristic band of isopropanol become visible. Most bands attributed to alkoxides disappeared after 90 minutes including the μ2-Al–OC vibration at 1033 cm^{-1} after 105 minutes. Complete hydrolysis

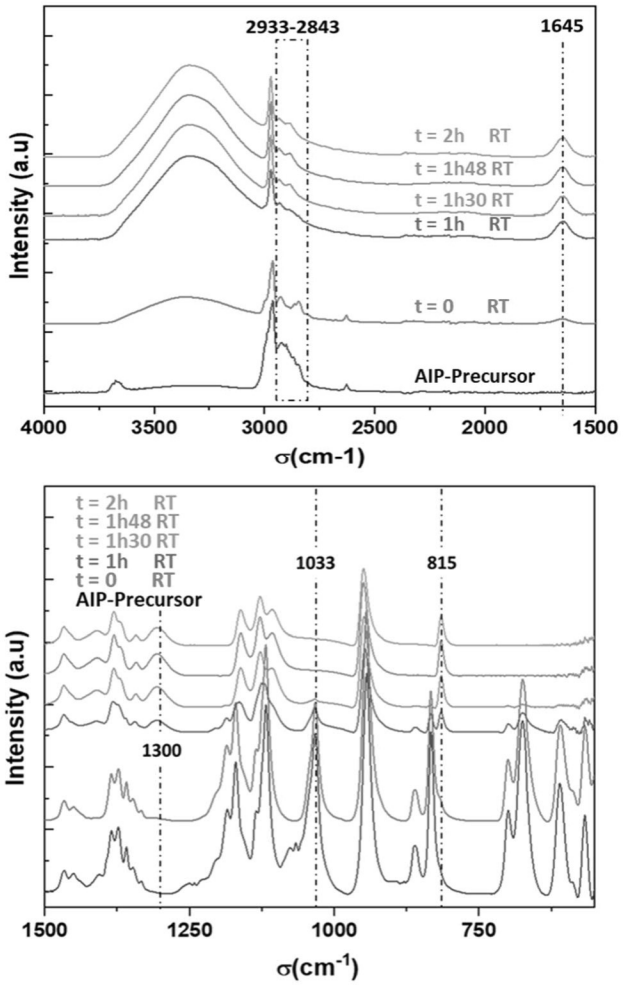

Fig. 3 Infrared spectra of RE_AlP_8_F samples as a function of time after reactive extrusion processing.

of AIP is considered to have taken place at this time. No more change is observed afterwards.

Study of condensation kinetics

The RE_AIP_8_F sample was analyzed by XRD after aging in air at room temperature and at different time intervals, from one hour to 28 hours (Fig. 4). No diffraction peaks from AIP is visible (reference AIP XRD patterns are provided in SI.2†),[66] confirming that most of AIP is either hydrolyzed (this is coherent with the FTIR data on hydrolysis kinetics) or not crystalline. The presence of very broad bands at diffraction angles close to those of boehmite materials means that extrudates are made of low-ordered boehmite. From one to three hours of aging, slow boehmite structuration of boehmite sheets is observed with the slow sharpening of boehmite diffraction peaks. From five hours of aging, the (020) diffraction peak characteristic of the stacking of boehmite sheets appears, meaning that the inorganic network starts its polymerization. This process goes on until no further evolution can be observed (after 28 hours of aging).

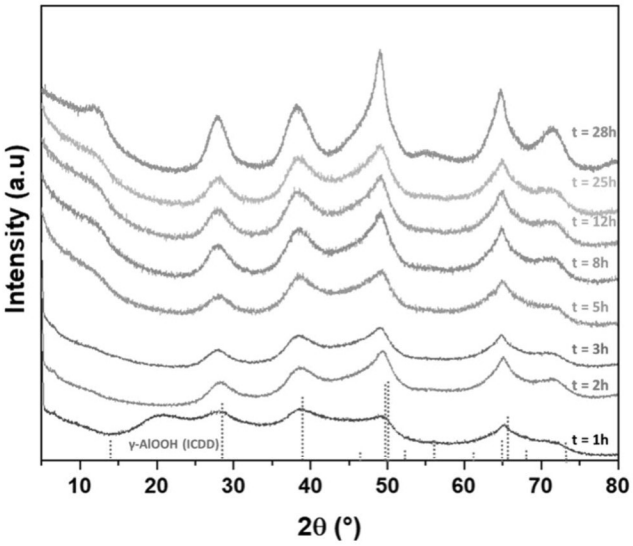

Fig. 4 XRD patterns of RE_AlP_8_F samples as a function of resting time at room temperature after extrusion.

Structural analysis of extrudates

For performing a reproducible structural study, four hours after synthesis we dried the samples under vacuum for removing the remaining water and alcohol molecules and compared XRD patterns of RE_AIP_6_D and RE_AIP_8_D as shown in Fig. 5. Both products show 6 broad peaks that can be indexed to the (020), (021), (130), (150), (132) and (152) characteristic plans of a nanometric boehmite phase.

The Scherrer equation was used to calculate boehmite crystallites dimensions over specific directions of (020), (021), and (130) (Table 1). RE_AIP_8_D and RE_AIP_6_D have very similar crystallite dimensions of less than 5 nm.[67] The aspect ratio of crystallites was calculated from d(020) and d(021). The result is

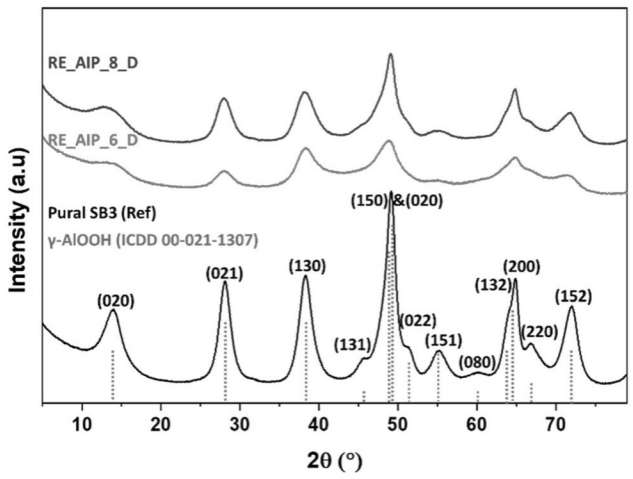

Fig. 5 XRD patterns of RE_AlP_8_D and RE_AlP_6_D samples. A commercial boehmite (Pural SB3) and peak indexation from the ICDD file are provided for comparison.

Table 1 RE_AIP_6_D and RE_AIP_8_D crystallite lengths in the *d*(020), *d*(021), and *d*(130) directions and aspect ratios calculated from *d*(020) and *d*(021). Taking into consideration that crystallite length is difficult to evaluate with precision, we added brackets on the last digit of the evaluation

Sample	$d_{(020)}$ (nm)	$d_{(021)}$ (nm)	$d_{(130)}$ (nm)	$d_{(020)}/d_{(021)}$
RE_AIP_6_D	2.(9)	4.(1)	3.(9)	0.7
RE_AIP_8_D	2.(4)	4.(7)	3.(7)	0.5

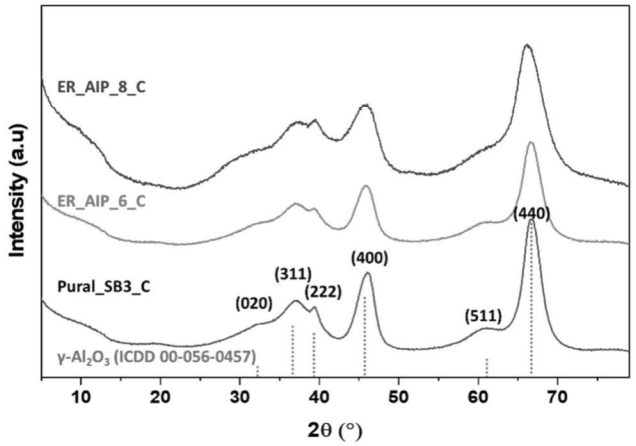

Fig. 6 XRD patterns of RE_AIP_8_C and RE_AIP_6_C samples. A commercial gamma alumina obtained by calcining the Pural SB3 reference boehmite and peak indexation from the ICDD file are provided for comparison.

equal to or below 0.7, showing that extrudates are made of ultra-small 2D sheet-like nanocrystals with a moderate aspect ratio.[67]

Tettenhorst *et al.*[68] compared the experimental XRD of boehmite powders with the calculated one. Their work shows that the d(020) reflection 2θ position gives information about crystallite's thickness for thin nanoparticles. They showed that the d(020) reflection slightly shifts below 14.6° for a crystallite thickness inferior to 3 crystal meshes (3.6 nm). Since the position of this peak in our materials is $2\theta_{(020)} < 14.0°$, the crystallite thickness can be assumed to be under 3.6 nm (less than three boehmite sheets in average), which is consistent with the thickness calculated by the Scherrer equation.

Samples calcined for 4 hours at 540 °C exhibit four main diffraction peaks indexed to the (311), (222), (400) and (440) planes, characteristic of a gamma alumina phase (Fig. 6).

TEM images of the RE_AIP_8_D sample (*cf.* Fig. 7) show that our materials consist of a homogeneous tangle of platelets with an average length of 50 nm (±20). It is possible to observe only few heterogeneous domains of a few hundred nanometers (Fig. SI.3†). From these TEM images, we can hypothesize that the presence of these domains is the signature of partially hydrolyzed AIP grains.

SEM analyses of calcined extrudates give an overview of the final structure at a near macroscopic scale (Fig. 8). For this analysis, each extrudate was broken into two pieces and the fracture was examined. On the one hand, RE_AIP_6_C extrudates exhibit a heterogeneous composite structure made of grains (size ranging from 1 to 15 micrometers) scattered within a continuous phase. Grains seem poorly cohesive with the continuous phase. Such a microstructure is likely to result from a lack of homogeneity of the reactive extrusion/shaping process and can be due to either (i) the unreacted alkoxide grains trapped within a partly reacted matrix after the extrusion process, and/or (ii) a problem of extrudate compacity resulting from inhomogeneous compression into the dye of the extruder. On the other hand, RE_AIP_8_C images show a homogeneous phase with no large particles (the long fracture line clearly visible on the pictures is due to the breaking of the extrudate).

Thus, it seems that the mechanical strength of our material is closely related to the phase homogeneity at the micrometer scale, the presence of large particles and holes favoring very probably the propagation of cracks. Whenever calcined extrudates are subjected to a very basic and qualitative mechanical test, crushing between fingers, RE_AIP_8_C is able to resist the pressure without breaking while RE_AIP_6_C is crushed to a

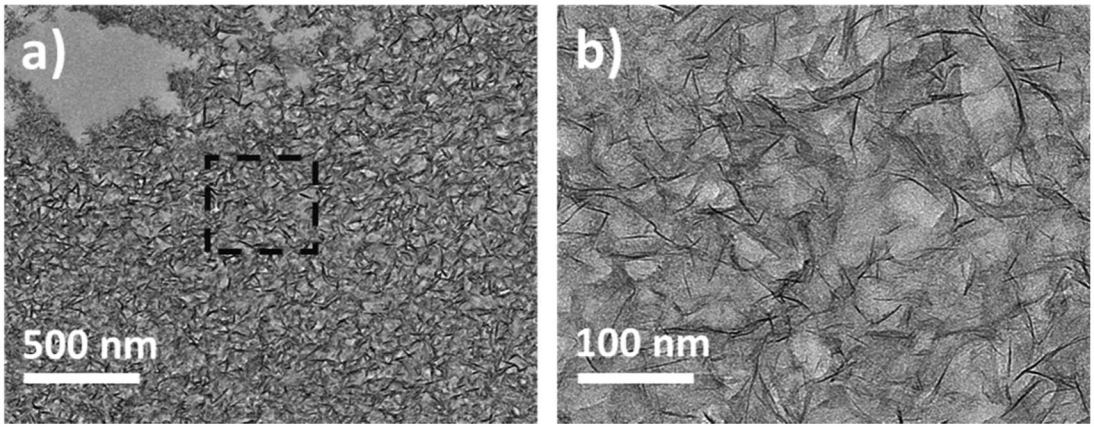

Fig. 7 Microtome TEM pictures of the RE_AIP_8_ D sample. (a) View at a large scale; (b) zoom-in image of the black square zone.

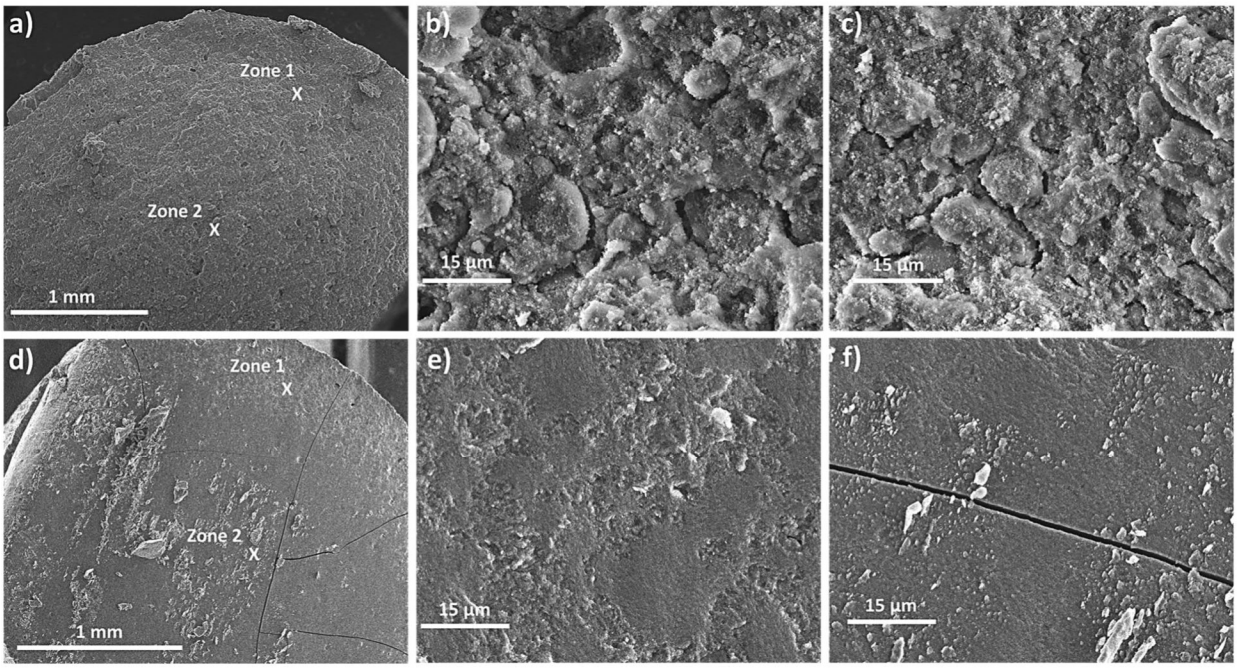

Fig. 8 SEM images of fractured extrudates: (a) RE_AIP_6_C extrudate; (b) RE_AIP_6_C zoom in zone 1 at the edge of the extrudate; (c) RE_AIP_6_C zoom in zone 2 in the middle of the extrudate; (d) RE_AIP_8_C extrudate; (e) RE_AIP_8_C zoom in zone 1 at the edge of the extrudate; and (f) RE_AIP_8_C zoom in zone 2 in the middle of the extrudate.

powder. To estimate the mechanical strength of RE_AIP_8_C compared to real industrial requirements, we performed a quantitative mechanical test of crushing strength called the "side crushing test". The strongest extrudates broke at 1.14 daN mm^{-1}. According to this mechanical test, their integrity is comparable to that of classical industrial extrudates prepared by a conventional kneading/extrusion process.[69] These preliminary results are of very high interest for they prove that extrudates prepared by reactive extrusion are already close to reaching industrial requirements. The understanding of reactivity mechanisms is likely to help us further improve the cohesion strength of our materials, thus their average value of crushing strength.

Reaction mechanisms

From a sol–gel chemistry point of view, the reactive medium being essentially granular AIP with a few droplets of water, and the hydrolysis reaction probably takes place in two steps. In the first step, the extrusion processing intimately mixes the newly added water and AIP grains so that water has little or no diffusion problems to reach the surface of the grains. At the AIP grain surface, hydrolysis starts with a high water/AIP molar ratio (higher than the average rate introduced), resulting in the formation of large aggregates of platelets. Rapidly, hydrolysis leads to the formation of isopropanol which slowly diffuses into AIP grains with the remaining water, creating a hydro-alcoholic front which propagates the hydrolysis reaction towards the center of AIP grains. As a consequence, one can assume that AIP grains are hydrolyzed progressively until they are consumed. The remaining domains observed in Fig. SI.3† are likely to be the very center of larger AIP grains partially hydrolyzed during the synthesis or/and AIP domains imperfectly mixed with water. From a chemical reaction point of view, the solvent-free hydrolysis and condensation of aluminum alkoxides follow the very specific pathway known for most metal alkoxides that form metal oxoalkoxo polymers of general formula $M^zO_{\left(\frac{z}{2}-\frac{x}{2}-\frac{y}{2}\right)}(OH)_x(OR)_y$.[47,70] The extra small dimensions of crystallites are characteristic of a massive nucleation process, followed by a very limited growth of crystals due to the very small diffusion coefficient of the reactant and product within a highly viscous matrix resulting from the absence of dispersion media (solvent). A second specificity of the solvent-free pathway is that no external heating of the reactant was needed for producing boehmite, while heating is most often used to obtain the same crystallographic phase in the presence of a solvent.[71] Yet, in our case, we must highlight that the hydrolysis step is very exothermic, so that the condensation step is in fact running in a hot environment (we monitored 43 °C with the external extruder thermocouple, meaning that no external heat is needed for the reactive extrusion of our samples). Hence, the result of our experiments is coherent with thermodynamics and the literature data highlighting that a warm environment favors the crystallization of boehmite.

Textural characterization of extrudates

We analyzed the textural properties of dried and calcined extrudates by nitrogen physisorption. The surface area, porous volume, and pore size distribution are listed in Table 2. All iso-

Table 2 RE_AIP_6_D and RE_AIP_8_D extrudate textural properties

Sample	S_{BET} (m^2 g^{-1})	V_p [a] (cm^3 g^{-1})	Pore size[b] (nm)
RE_AIP_6_D	308	1.0	11.2
RE_AIP_6_C	228	1.0	12.2
RE_AIP_8_D	391	1.7	15.2
RE_AIP_8_C	337	1.9	18.0

[a] Porous volume was taken at P/P_0 = 0.99. [b] Pore size distribution was estimated with the BJH model at the desorption branch.

therms (Fig. SI.4†) exhibit hysteresis loops characteristic of wedge-shaped pores,[72] which is consistent with TEM observations. RE_IPA_6_D has a specific surface area of 308 m^2 g^{-1}, a porous volume of 1.0 cm^3 g^{-1} and a pore size distribution at desorption centered at 11.2 nm. RE_AIP_8_D extrudates present a higher surface area (391 m^2 g^{-1}) and porous volume (1.7 cm^3 g^{-1}), as well as a larger pore size distribution (15.2 nm) compared to RE_AIP_6_D. All pore size distributions are asymmetric and broad, extending down to 4 nm. After calcination, RE_AIP_6_C shows an important decrease in the surface area, falling down to 228 m^2 g^{-1}, while the porous volume remained stable at 1.0 cm^3 g^{-1}, and the mean pore size distribution increased slightly to 12.2 nm. The same trend has been observed for RE_AIP_8_C. It shows a slight decrease in the surface area (337 m^2 g^{-1}), an increase in the pore volume (1.9 cm^3 g^{-1}) and a larger average pore size (18 nm) (Fig. SI.5†).

Overall, RE_AIP_8_C presents remarkable textural properties, which are comparable or even higher than gamma alumina obtained from salt co-precipitation[73] and complex syntheses[74] (for which no extrudate shaping is reported).

Catalytic tests

Calcined extrudates were tested in the gas phase dehydration of ethanol, and compared with a commercial γ-alumina powder with a surface area of 100 m^2 g^{-1} (commonly used industrially for such a reaction).[75] For comparison, we also used boehmite powders prepared with the same solvent-free reaction but made with a steel anchor in a polypropylene bottle. The resulting materials were then shaped using a usual kneading, peptization, neutralization and extrusion pathway in order to determine the influence of the shaping process on the catalytic performance. We obtained in this way two other types of extrudates, KE_ASB_6_C and KE_AIP_5_C, with surface areas of 314 and 302 m^2 g^{-1}, respectively (see full characterization in SI.6†). This hybrid alternative method (solvent-free boehmite synthesis followed by regular kneading/extrusion) uses more than one device but it is still attractive from a sustainability point of view because it uses no solvent and produces no liquid waste.

Catalytic tests were performed on crushed extrudates. Interestingly, the ethanol conversion is already very significant at 210 °C (higher than 40% for our materials) and even reaches 75% for the KE_ASB_6_C sample (Fig. 9). As expected, the conversion increases with raising temperature; it is higher than 80% at 255 °C for all materials prepared by solvent-free syntheses and reaches 100% at 315 °C (while commercial γ-Al_2O_3 does not reach full conversion at this temperature). Major products obtained are diethyl ether and ethylene with the carbon balance ranging between 95 and 109% (98–103% in the majority of experiments). Acetaldehyde and butene (products of ethanol dehydrogenation and ethylene dimerization, respectively) were observed at 255 and 315 °C in

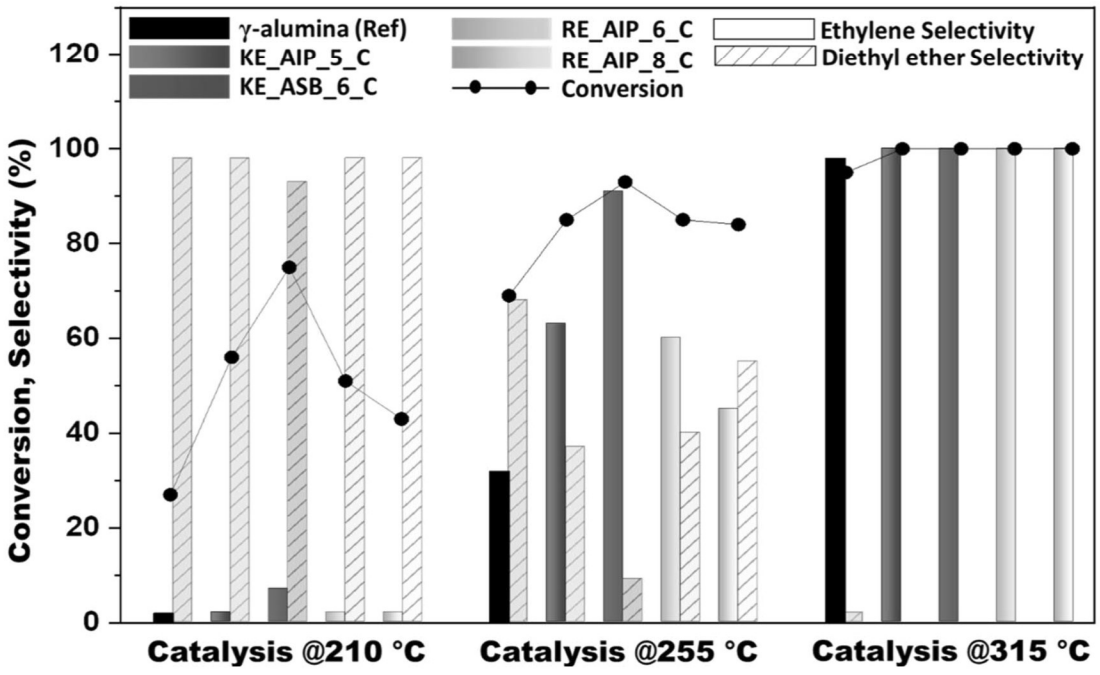

Fig. 9 Ethanol dehydration conversion at different catalysis temperatures Vs ethylene and diethyl ether selectivity.

minute amounts (<1%). Higher temperatures favored the production of ethylene in agreement with the reaction thermodynamics and the literature.[76–79] From a selectivity point of view, it can be observed that the ethylene selectivity at 255 °C is always higher than 40% and even reaches an impressive 91% for the KE_ASB_6_C sample. This point is to compare with the reference γ-alumina which exhibits only 32% of selectivity at 255 °C. In all cases, the catalysts were very stable during these analyses, similar to other reports on alumina, as it can be seen in Fig. SI.7.†[76,77]

The reference γ-alumina showed similar catalytic behavior to previously reported data on non-shaped commercial alumina and amorphous silica-alumina catalysts.[76,80–83] For example, Phung *et al.* reported a stepwise increase of ethanol conversion from 2–21% to 72–98% when changing temperatures from 200 to 300 °C at WHSV = 1.43 h^{-1} over commercial alumina catalysts prepared by various methods (flame hydrolysis; precipitation of Al salts; synthesized from Al alkoxides). Commercial silica-alumina showed similar catalytic behavior.[76,82] The materials produced by solvent-free synthesis and shaped as extrudates after kneading-extrusion or directly by reactive extrusion exhibited comparable or better dehydration activity. More globally, a simple selectivity and conversion comparison with the results of the literature showed that our results are comparable with those of pure inorganic and hybrid aluminosilicate catalysts obtained by an advanced non-hydrolytic sol–gel method (ethanol conversion~85%, selectivity to ethylene 60–80% at 240 °C and identical WHSV).[59,80,84] The HZSM-5 molecular sieve containing strong Brønsted acid sites showed a higher catalytic activity (ethanol conversion~90%, selectivity to ethylene 90% at 240 °C and WHSV = 17.5 h^{-1});[80] however it suffers from rapid deactivation by coking.[80,81] Although a precise performance evaluation of our samples would need a dedicated study at low conversion (less than 20%) and acidity measurement tests, the materials presented herein exhibit high potential for catalytic applications, not only from the point of view of catalytic performance, but also from a sustainability point of view as discussed in the following section.

Atoms and energy metrics

We made an attempt to compare the one-step reactive extrusion approach with a boehmite synthesis approach using precipitation at a high concentration of reactants (which is a representative of industrial reality).[34] In this section, we calculated atom and energy consumptions, and estimated the *E*-factor (total mass of waste divided by the produced mass of the catalyst) and space time yield of production (the mass of final product obtained per cubic meter of the reactor in one day). We highlight here that the *E*-factor usually does not consider water in its calculation. The pertinence of this point can be debated for all liquid waste dissolved in water are not easily eliminated and water recycling costs time and energy. Also, considering that water rarefaction is considered by the United Nations as one of the seventeen challenges to solve for the coming century, we decided to consider water and thus also calculate what is commonly referred to as the "complete *E*-factor" (c*E*-factor).[14] We compared three scenarios considering only the preparation of dry boehmite. For this comparison, we excluded calcination for it is the same for materials prepared by reactive extrusion and precipitation. We highlight that, while reactive extrusion integrates a shaping step, the precipitation method requires additional kneading and shaping steps (*i.e.* two more tools with their energy consumption and longer preparation time). These additional costs were not included in the energetic comparison presented below.

The first scenario is the conventional synthesis method in which aluminum salts are precipitated in water, then filtered, washed and dried. In this case, we considered the use of 0.75 mol l^{-1} of aluminum salt in water and two possible precipitation temperatures, 30 and 85 °C. For washing, we considered that three times the reaction volume of solvent at ambient temperature is required (this step is usually not described in the literature but from salt counterion dilution calculations, three washings are likely to be a minimum). The second scenario is the equivalent of the first one, pushed at its theoretical limit, that is, we consider that the aqueous solution of aluminum nitrate salt is saturated before the reaction. This was calculated for determining the theoretical limit of the precipitation approach. The third scenario is the case of the reactive extrusion presented herein, requiring no energy input for heating (the exothermicity of the reaction is enough for promoting boehmite crystallization, as demonstrated above).

The energy consumption of devices is not included in the calculations. Similarly it is considered that precipitation reactors are perfectly isolated from a thermal point of view. We considered only the energy required for the chemical reaction and washing (heating of water). The powder drying energy consumption was calculated by considering only the vaporization enthalpy of the remaining solvent (the wet cake of boehmite typically contains in between 84% and 93% of water by weight before drying,[42,43] and isopropanol for reactive extrusion). We summarized the comparison in Table 3.

The comparison of water consumption between precipitation and solvent-free reactive extrusion methods highlights immediately the huge advantage of reactive extrusion which simply does not use any solvent. The *E*-factor calculated (more representative of atom consumption at the industrial scale) is more than two times higher for the precipitation method if we do not consider water. Yet, using chemical grade water (either purified or recycled) has a cost. The more realistic comparison based on the c*E*-factors yields a value of 110, that is, nearly 19 times higher than that of the reactive extrusion method. When compared with the theoretical limit of the precipitation method (that is starting from a salt-saturated solution), the c*E*-factor of reactive extrusion is still 8 times lower, highlighting the very significant sustainability gain that can be achieved by using reactive extrusion processing. From an energy consumption point of view, the precipitation method consumes energy for heating the precipitation solution and evaporating the remaining solvent from the final boehmite. Reactive extrusion consumes 12 times less energy. This calculation does not take in consideration the energetic consumption of devices used

Table 3 Atom and energy consumptions, *E*-factor and c*E*-factor are calculated for a conventional precipitation, a fictive ideal precipitation, and for the reactive extrusion processes. Values are given for the production of 1 kg of AlOOH

	Reference precipitation	Theoretical limit of precipitation	Reactive extrusion
Atoms			
Water (kg)	102.4	41.9	2.39
Aluminium salts (mol)	16.6	16.6	—
Aluminium alkoxides (mol)			16.6
NH_4OH (kg)	1.4	1.4	—
Energy			
Solvent heating (MJ)	4.3[a] to 27.8[b]	1.7[a] to 11.4[b]	—
Vaporization (MJ)	21.9	21.9	1.9
E-Factor	7.5[c]	7.5[c]	3.4
c*E*-Factor	110.0	49.5	5.8

[a] Precipitation temperature is 30 °C. [b] Precipitation temperature is 85 °C. [c] Hydration water of the salt was removed for this calculation.

for mixing, kneading, filtering and washing of the precipitation approach so that the advantage of reactive extrusion is actually underestimated.

Altogether, from an industrial point of view, the space time yield (STY) is another useful indicator. Intrinsically, reactive extrusion using the mass reaction with no solvent reaches a very high STY. In the present case, the calculation can be performed in two ways. If one considers that the volume of the twin screw of the extruder is a part of the volume of the reactor, the STY of our process is 11 525 kg m^{-3} day^{-1}. If one considers that the volume of the used reactor is the volume of reactants only, the STY is five time higher. We did not find in the literature any appropriate estimation of the STY for the standard manufacture of boehmite by precipitation. Yet, we can compare with other materials prepared by precipitation such as MOFs. The optimized BASF production of aluminium fumarate is amongst the best ever reported in the literature with a STY of only 3600 kg m^{-3} day^{-1}.[85]

Finally, we did not discuss the production cost as it depends very much on the industrial environment, manpower cost, investment cost, maintenance cost and chemical reactant cost. The latter is difficult to estimate at the industrial scale as it depends on negotiations. While Al alkoxides are significantly more expensive than their chloride or nitrate counterparts, we can very probably balance the reactant cost difference with the huge gains in energy, manpower and maintenance costs. Continuous reactive extrusion processing, using only one device from the chemical reaction to the final shaping of the catalyst, is likely a realistic alternative to the batch precipitation method using several devices with a global improved environmental footprint.

Conclusion

To summarize, we presented a new integrated method for the green synthesis and shaping of high surface area boehmite supports. The obtained materials are successfully prepared in one step *via* a solvent-free pathway using aluminium alkoxides that requires no sacrificial organic pore generating agents such as surfactants or polymers, no washing, and no filtration, and produces no liquid waste. Upon calcination, high surface area γ-alumina extrudates are readily obtained. Thus, this solvent-free synthesis strategy can be easily implemented for the industrial production of heterogeneous catalysts or supports. We proved that the shaped γ-alumina materials prepared through reactive extrusion exhibit high ethanol dehydration catalytic properties, competing with similar materials. The decisive advantage of this innovative method is the drastic intensification of the production process, featuring sustainability metrics (atom economy, energy consumption, *E*-factor, and c*E*-factor) that are outstanding, as compared to those of the conventional precipitation method. Indeed, by comparison with a standard production method – even if using highly concentrated aqueous salt solutions – the reactive extrusion process uses one extruder for replacing several devices (used for mixing, filtering, washing, and kneading), and it completely eliminates all filtration and, if salt precursors are used, washing steps. Concomitantly, we replaced a batch production process by a continuous production process, removing the need for heating a large volume of solvents (the hydrolysis of the reactant produces enough energy for boehmite synthesis).

As this last aspect also allows saving a lot of atoms, energy, and manpower, we do believe that the strategy presented here paves the way towards the sustainable industrial production of such nanomaterials. Such a one step-one tool process opens new interesting ways for shaping porous materials synthesis since it may subsequently be reproduced for many other oxides as far as alkoxides are available. Due to the great versatility of the process, the preparation of more complex materials such as mixed oxides or metal-supported oxide catalysts can also be envisaged.

Author contributions

Pierre-Igor Dassie performed the materials synthesis, characterization studies, bibliographic studies and manuscript writing; Ryma Haddad performed the materials synthesis, characterization studies, bibliographic studies and manuscript writing; Maud Lenez performed the materials synthesis and characterization studies; Alexandra Chaumonnot performed the conceptual conception, student management, data interpretation and manuscript writing; Malika Boualleg performed the conceptual conception, student management, data interpretation and manuscript writing; Patrick Legriel performed the electron microscopy experiments; Ales Styskalik performed the catalytic tests experiments and data treatments; Bernard Haye performed the microtome cut of the sample; Mohamed Selmane performed the XRD analyses and modelizations; Damien P. Debecker performed the catalytic studies, conception and interpretations, management, and manuscript writing; Clement Sanchez performed the conceptual con-

ception, data interpretation and manuscript writing; Corinne Chaneac performed the conceptual conception, student management, data interpretation and manuscript writing; Cedric Boissiere performed the conceptual conception, student management, data interpretation and manuscript writing.

Conflicts of interest

There are no conflicts of interest between the authors or the institutions of the study.

Acknowledgements

This work was supported by IFPEN and by ED397 Doctoral School Materials Physics/Chemistry of Sorbonne University.

References

1 T. R. Reina, J. A Odriozola, Heterogeneous Catalysis for Energy Applications, 2020. ebook collection, ECCC Environmental eBooks 1968-2022, DOI: **10.1039/9781788019576**.

2 J. R. H. Ross, Chapter 12 – Catalytic Reactions Involving Syngas, Hydrogen, or Carbon Monoxide for the Production of Intermediates and Chemicals, in *Contemporary Catalysis*, ed. J. R. H. Ross, Elsevier, Amsterdam, 2019, pp. 273–290. DOI: **10.1016/B978-0-444-63474-0.00012-6**.

3 *Environmental Catalysis*, ed. V. H. Grassian, CRC Press, Boca Raton, 2005. DOI: **10.1201/9781420027679**.

4 S. Morales-Torres, L. M. Pastrana-Martínez and F. J. Maldonado-Hódar, Carbon Nanomaterials for Air and Water Remediation, in *Nanostructured Catalysts for Environmental Applications*, ed. M. Piumetti and S. Bensaid, Springer International Publishing, Cham, 2021, pp. 331–365. DOI: **10.1007/978-3-030-58934-9_12**.

5 M. J. Marin Figueredo, M. Piumetti, S. Bensaid, D. Fino and R. Nunzio, Catalytic Oxidation of Volatile Organic Compounds over Porous Manganese Oxides Prepared via Sol-Gel Method, in *Nanostructured Catalysts for Environmental Applications*, ed. M. Piumetti and S. Bensaid, Springer International Publishing, Cham, 2021, pp. 59–78. DOI: **10.1007/978-3-030-58934-9_2**.

6 M. J. Ndolomingo, N. Bingwa and R. Meijboom, Review of Supported Metal Nanoparticles: Synthesis Methodologies, Advantages and Application as Catalysts, *J. Mater. Sci.*, 2020, **55**(15), 6195–6241, DOI: **10.1007/s10853-020-04415-x**.

7 F. Ferlin, S. Santoro, L. Ackermann and L. Vaccaro, Heterogeneous C–H Alkenylations in Continuous-Flow: Oxidative Palladium-Catalysis in a Biomass-Derived Reaction Medium, *Green Chem.*, 2017, **19**(11), 2510–2514, DOI: **10.1039/C7GC01103B**.

8 M. Irfan, T. N. Glasnov and C. O. Kappe, Heterogeneous Catalytic Hydrogenation Reactions in Continuous-Flow Reactors, *ChemSusChem*, 2011, **4**(3), 300–316, DOI: **10.1002/cssc.201000354**.

9 J. R. H. Ross, Chapter 7 - Large-Scale Catalytic Reactors, in *Heterogeneous Catalysis*, ed. J. R. H. Ross, Elsevier, Amsterdam, 2012, pp. 143–169. DOI: **10.1016/B978-0-444-53363-0.10007-6**.

10 H. Touati, S. Valange, M. Reinholdt, C. Batiot-Dupeyrat, J.-M. Clacens and J.-M. Tatibouët, Low Temperature Catalytic Oxidation of Ethanol Using Ozone over Manganese Oxide-Based Catalysts in Powdered and Monolithic Forms, *Catalysts*, 2022, **12**(2), 172, DOI: **10.3390/catal12020172**.

11 L. Lakiss, J.-P. Gilson, V. Valtchev, S. Mintova, A. Vicente, A. Vimont, R. Bedard, S. Abdo and J. Bricker, Zeolites in a Good Shape: Catalyst Forming by Extrusion Modifies Their Performances, *Microporous Mesoporous Mater.*, 2020, **299**, 110114, DOI: **10.1016/j.micromeso.2020.110114**.

12 V. Middelkoop, A. Vamvakeros, D. de Wit, S. D. M. Jacques, S. Danaci, C. Jacquot, Y. de Vos, D. Matras, S. W. T. Price and A. M. Beale, 3D Printed Ni/Al_2O_3 Based Catalysts for CO2 Methanation - a Comparative and Operando XRD-CT Study, *J. CO2 Util.*, 2019, **33**, 478–487, DOI: **10.1016/j.jcou.2019.07.013**.

13 O. A. Alimi, T. B. Ncongwane and R. Meijboom, Design and Fabrication of a Monolith Catalyst for Continuous Flow Epoxidation of Styrene in Polypropylene Printed Flow Reactor, *Chem. Eng. Res. Des.*, 2020, **159**, 395–409, DOI: **10.1016/j.cherd.2020.04.025**.

14 D. P. Debecker, K. Kuok (Mimi) Hii, A. Moores, L. M. Rossi, B. Sels, D. T. Allen and B. Subramaniam, Shaping Effective Practices for Incorporating Sustainability Assessment in Manuscripts Submitted to ACS Sustainable Chemistry & Engineering: Catalysis and Catalytic Processes, *ACS Sustainable Chem. Eng.*, 2021, **9**(14), 4936–4940, DOI: **10.1021/acssuschemeng.1c02070**.

15 B. V. Vora, Development of Dehydrogenation Catalysts and Processes, *Top. Catal.*, 2012, **55**(19), 1297–1308, DOI: **10.1007/s11244-012-9917-9**.

16 A. Abdulrasheed, A. A. Jalil, Y. Gambo, M. Ibrahim, H. U. Hambali and M. Y. Shahul Hamid, A Review on Catalyst Development for Dry Reforming of Methane to Syngas: Recent Advances, *Renewable Sustainable Energy Rev.*, 2019, **108**, 175–193, DOI: **10.1016/j.rser.2019.03.054**.

17 G. Bagnato, A. Sanna, E. Paone and E. Catizzone, Recent Catalytic Advances in Hydrotreatment Processes of Pyrolysis Bio-Oil, *Catalysts*, 2021, **11**(2), 157, DOI: **10.3390/catal11020157**.

18 F. Feng, Z. Shang, L. Wang, X. Zhang, X. Liang and Q. Wang, Structure-Sensitive Hydro-Conversion of Oleic Acid to Aviation-Fuel-Range-Alkanes over Alumina-Supported Nickel Catalyst, *Catal. Commun.*, 2020, **134**, 105842, DOI: **10.1016/j.catcom.2019.105842**.

19 H. Hattori and Y. Ono, Catalysts and Catalysis for Acid–Base Reactions, in *Metal Oxides in Heterogeneous Catalysis*, ed. J. C. Védrine, Metal Oxides, Elsevier, 2018, ch. 4, pp. 133–209. DOI: **10.1016/B978-0-12-811631-9.00004-1**.

20 R. Wischert, P. Laurent, C. Copéret, F. Delbecq and P. Sautet, γ-Alumina: The Essential and Unexpected Role of Water for the Structure, Stability, and Reactivity of "Defect" Sites, *J. Am. Chem. Soc.*, 2012, **134**(35), 14430–14449, DOI: **10.1021/ja3042383**.

21 P. Euzen, P. Raybaud, X. Krokidis, H. Toulhoat, J.-L. Le Loarer, J.-P. Jolivet and C. Froidefond, Alumina, in *Handbook of Porous Solids*, John Wiley & Sons, Ltd, 2002, pp. 1591–1677. DOI: **10.1002/9783527618286.ch23b**.

22 B. C. Lippens, *Structure and Texture of Aluminas*. 1961.

23 A. Valette, *Amélioration Des Propriétés Texturales de l'alumine Par Le Contrôle de l'état d'agrégation de Bâtonnets*. These kde doctorat, Sorbonne université, 2019. **https://www.theses.fr/2019SORUS395** (accessed 2023-01-31).

24 G. G. Hritz, B. E. Leach and D. J. Royer, Aluminum Oxyde Extrudate and Process for ITS Manufacturing. DE2237861A1, 1973. **https://patents.google.com/patent/DE2237861A1/en** (accessed 2022-10-14).

25 P. J. V. D. Brink, R. J. Dogterom and C. M. A. M. Mesters, Method of Manufacturing a Catalyst. US7582588B2, 2009. **https://patents.google.com/patent/US7582588B2/en?oq=V.D.+Brink%2c+Method+of+manufacturing+a+catalyst%2c+US+patent+7582588%2c+(2009)** (accessed 2022-10-14).

26 B. E. Yoldas, Hydrolysis of Aluminium Alkoxides and Bayerite Conversion, *J. Appl. Chem. Biotechnol.*, 1973, **23**(11), 803–809, DOI: **10.1002/jctb.5020231103**.

27 T. Adschiri, K. Kanazawa and K. Arai, Rapid and Continuous Hydrothermal Synthesis of Boehmite Particles in Subcritical and Supercritical Water, *J. Am. Ceram. Soc.*, 1992, **75**(9), 2615–2618, DOI: **10.1111/j.1151-2916.1992.tb05625.x**.

28 K. Okada, T. Nagashima, Y. Kameshima, A. Yasumori and T. Tsukada, Relationship between Formation Conditions, Properties, and Crystallite Size of Boehmite, *J. Colloid Interface Sci.*, 2002, **253**(2), 308–314, DOI: **10.1006/jcis.2002.8535**.

29 T. Kotanigawa, M. Yamamoto, M. Utiyama, H. Hattori and K. Tanabe, The Influence of Preparation Methods on the Pore Structure of Alumina, *Appl. Catal.*, 1981, **1**(3), 185–200, DOI: **10.1016/0166-9834(81)80006-1**.

30 R. R. Toledo, V. R. Santoyo, C. D. M. Sánchez and M. M. Rosales, Effect of Aluminum Precursor on Physicochemical Properties of Al_2O_3 by Hydrolysis/Precipitation Method, *Nova Sci.*, 2018, **10**(20), 83–99, DOI: **10.21640/ns.v10i20.1217**.

31 S. Ramanathan, S. K. Roy, R. Bhat, D. D. Upadhyaya and A. R. Biswas, Alumina Powders from Aluminium Nitrate-Urea and Aluminium Sulphate-Urea Reactions—The Role of the Precursor Anion and Process Conditions on Characteristics, *Ceram. Int.*, 1997, **23**(1), 45–53, DOI: **10.1016/0272-8842(95)00139-5**.

32 R. Brusasco, J. Gnassi, C. Tatian, J. Baglio, K. Dwight and A. Wold, Preparation and Characterization of Fibrillar Boehmite and γ-Al_2O_3, *Mater. Res. Bull.*, 1984, **19**(11), 1489–1496, DOI: **10.1016/0025-5408(84)90263-0**.

33 E. Morgado, Y. L. Lam and L. F. Nazar, Formation of Peptizable Boehmites by Hydrolysis of Aluminum Nitrate in Aqueous Solution, *J. Colloid Interface Sci.*, 1997, **188**(2), 257–269, DOI: **10.1006/jcis.1997.4780**.

34 F. Karouia, M. Boualleg, M. Digne and P. Alphonse, Control of the Textural Properties of Nanocrystalline Boehmite (γ-AlOOH) Regarding Its Peptization Ability, *Powder Technol.*, 2013, **237**, 602–609, DOI: **10.1016/j.powtec.2012.12.054**.

35 S. Ozkan, H. Gevgilili, D. M. Kalyon, J. Kowalczyk and M. Mezger, Twin-Screw Extrusion of Nano-Alumina–Based Simulants of Energetic Formulations Involving Gel-Based Binders, *J. Energ. Mater.*, 2007, **25**(3), 173–201, DOI: **10.1080/07370650701399320**.

36 D. P. Debecker, C. Boissière, G. Laurent, S. Huet, P. Eliaers, C. Sanchez and R. Backov, First Acidic Macro-Mesocellular Aluminosilicate Monolithic Foams "SiAl(HIPE)" and Their Catalytic Properties, *Chem. Commun.*, 2015, **51**(74), 14018–14021, DOI: **10.1039/C5CC05328E**.

37 S. Y. Devyatkov, A. A. Zinnurova, A. Aho, D. Kronlund, J. Peltonen, N. V. Kuzichkin, N. V. Lisitsyn and D. Y. Murzin, Shaping of Sulfated Zirconia Catalysts by Extrusion: Understanding the Role of Binders, *Ind. Eng. Chem. Res.*, 2016, **55**(23), 6595–6606, DOI: **10.1021/acs.iecr.6b00820**.

38 D. Y. Murzin, *Engineering Catalysis*, De Gruyter, 2020. DOI: **10.1515/9783110614435**.

39 M. Digne, P. Sautet, P. Raybaud, H. Toulhoat and E. Artacho, Structure and Stability of Aluminum Hydroxides: A Theoretical Study, *J. Phys. Chem. B*, 2002, **106**(20), 5155–5162, DOI: **10.1021/jp014182a**.

40 S. J. Smith, S. Amin, B. F. Woodfield, J. Boerio-Goates and B. J. Campbell, Phase Progression of γ-Al_2O_3 Nanoparticles Synthesized in a Solvent-Deficient Environment, *Inorg. Chem.*, 2013, **52**(8), 4411–4423, DOI: **10.1021/ic302593f**.

41 J. F. Le Page, *Applied Heterogeneous Ca.*, Editions OPHRYS, 1987.

42 R. Lafficher, *Nouveau procédé de précipitation pour la synthèse d'alumine. phdthesis*, Université de Lyon, 2016. **https://tel.archives-ouvertes.fr/tel-01425446** (accessed 2022-07-22).

43 R. Lafficher, M. Digne, F. Salvatori, M. Boualleg, D. Colson and F. Puel, Ammonium Aluminium Carbonate Hydroxide NH4Al(OH)2CO3 as an Alternative Route for Alumina Preparation: Comparison with the Classical Boehmite Precursor, *Powder Technol.*, 2017, **320**, 565–573, DOI: **10.1016/j.powtec.2017.07.080**.

44 I. Manas-Zloczower, *Mixing and Compounding of Polymers: Theory and Practice*, Hanser, 2009.

45 M. Lambla, Reactive Extrusion, in *Rheological Fundamentals of Polymer Processing*, ed. J. A. Covas, J. F. Agassant, A. C. Diogo, J. Vlachopoulos and K. Walters, NATO ASI Series, Springer Netherlands, Dordrecht, 1995, pp. 437–454. DOI: **10.1007/978-94-015-8571-2_20**.

46 D. Crawford, J. Casaban, R. Haydon, N. Giri, T. McNally and S. L. James, Synthesis by Extrusion: Continuous, Large-Scale Preparation of MOFs Using Little or No Solvent, *Chem. Sci.*, 2015, **6**(3), 1645–1649, DOI: **10.1039/C4SC03217A**.

47 J. Livage, M. Henry and C. Sanchez, Sol-Gel Chemistry of Transition Metal Oxides, *Prog. Solid State Chem.*, 1988, **18**(4), 259–341, DOI: **10.1016/0079-6786(88)90005-2**.

48 M. Nguefack, A. F. Popa, S. Rossignol and C. Kappenstein, Preparation of Alumina through a Sol–Gel Process. Synthesis, Characterization, Thermal Evolution and Model of Intermediate Boehmite, *Phys. Chem. Chem. Phys.*, 2003, **5**(19), 4279–4289, DOI: **10.1039/B306170A**.

49 W. Lueangchaichaweng, B. Singh, D. Mandelli, W. A. Carvalho, S. Fiorilli and P. P. Pescarmona, High Surface Area, Nanostructured Boehmite and Alumina Catalysts: Synthesis and Application in the Sustainable Epoxidation of Alkenes, *Appl. Catal., A*, 2019, **571**, 180–187, DOI: **10.1016/j.apcata.2018.12.017**.

50 M. May, J. Navarrete, M. Asomoza and R. Gomez, Tailored Mesoporous Alumina Prepared from Different Aluminum Alkoxide Precursors, *J. Porous Mater.*, 2007, **14**(2), 159–164, DOI: **10.1007/s10934-006-9020-3**.

51 A. Rajaeiyan and M. M. Bagheri-Mohagheghi, Comparison of Sol-Gel and Co-Precipitation Methods on the Structural Properties and Phase Transformation of γ and α-Al_2O_3 Nanoparticles, *Adv. Manuf.*, 2013, **1**(2), 176–182, DOI: **10.1007/s40436-013-0018-1**.

52 B. Huang, C. H. Bartholomew, S. J. Smith and B. F. Woodfield, Facile Solvent-Deficient Synthesis of Mesoporous γ-Alumina with Controlled Pore Structures, *Microporous Mesoporous Mater.*, 2013, **165**, 70–78, DOI: **10.1016/j.micromeso.2012.07.052**.

53 B. Huang, C. H. Bartholomew and B. F. Woodfield, Facile Structure-Controlled Synthesis of Mesoporous γ-Alumina: Effects of Alcohols in Precursor Formation and Calcination, *Microporous Mesoporous Mater.*, 2013, **177**, 37–46, DOI: **10.1016/j.micromeso.2013.04.013**.

54 B. Huang, C. H. Bartholomew and B. F. Woodfield, Facile Synthesis of Mesoporous γ-Alumina with Tunable Pore Size: The Effects of Water to Aluminum Molar Ratio in Hydrolysis of Aluminum Alkoxides, *Microporous Mesoporous Mater.*, 2014, **183**, 37–47, DOI: **10.1016/j.micromeso.2013.09.007**.

55 S. J. Smith, B. Huang, S. Liu, Q. Liu, R. E. Olsen, J. Boerio-Goates and B. F. Woodfield, Synthesis of Metal Oxide Nanoparticles via a Robust "Solvent-Deficient" Method, *Nanoscale*, 2014, **7**(1), 144–156, DOI: **10.1039/C4NR04964K**.

56 J. Oh, H. B. Bathula, J. H. Park and Y.-W. Suh, A Sustainable Mesoporous Palladium-Alumina Catalyst for Efficient Hydrogen Release from N-Heterocyclic Liquid Organic Hydrogen Carriers, *Commun. Chem.*, 2019, **2**(1), 1–10, DOI: **10.1038/s42004-019-0167-7**.

57 R. M. Kore and B. J. Lokhande, A Robust Solvent Deficient Route Synthesis of Mesoporous Fe2O3 Nanoparticles as Supercapacitor Electrode Material with Improved Capacitive Performance, *J. Alloys Compd.*, 2017, **725**, 129–138, DOI: **10.1016/j.jallcom.2017.07.145**.

58 B. F. Woodfield, S. Liu, J. Boerio-Goates, Q. Liu and S. J. Smith, Preparation of Uniform Nanoparticles of Ultra-High Purity Metal Oxides, Mixed Metal Oxides, Metals, and Metal Alloys, US8211388B2, 2012. **https://patents.google.com/patent/US8211388B2/en?oq=US8211388** (accessed 2022-03-08).

59 A. Styskalik, V. Vykoukal, L. Fusaro, C. Aprile and D. P. Debecker, Mildly Acidic Aluminosilicate Catalysts for Stable Performance in Ethanol Dehydration, *Appl. Catal., B*, 2020, **271**, 118926, DOI: **10.1016/j.apcatb.2020.118926**.

60 A. D. Cross, *An Introduction to Practical Infra-Red Spectroscopy*, Butterworths, 1964.

61 B. Smith, *The Infrared Spectra of Polymers V: Epoxies*. 2022..

62 F. A. D. Battaglin, R. S. Hosokawa, N. C. da Cruz, L. Caseli, E. C. Rangel, T. F. da Silva and M. H. Tabacniks, Innovative Low Temperature Plasma Approach for Deposition of Alumina Films, *Mater. Res.*, 2014, **17**, 1410–1419, DOI: **10.1590/1516-1439.283514**.

63 A. B. Kiss, G. Keresztury and L. Farkas, Raman and i.r. Spectra and Structure of Boehmite (γ-AlOOH). Evidence for the Recently Discarded D172 h Space Group, *Spectrochim. Acta, Part A*, 1980, **36**(7), 653–658, DOI: **10.1016/0584-8539(80)80024-9**.

64 C. Morterra and G. Magnacca, A Case Study: Surface Chemistry and Surface Structure of Catalytic Aluminas, as Studied by Vibrational Spectroscopy of Adsorbed Species, *Catal. Today*, 1996, **27**(3), 497–532, DOI: **10.1016/0920-5861(95)00163-8**.

65 C. G. Barraclough, D. C. Bradley, J. Lewis and I. M. Thomas, 510. The Infrared Spectra of Some Metal Alkoxides, Trialkylsilyloxides, and Related Silanols, *J. Chem. Soc. Resumed*, 1961, 2601–2605, DOI: **10.1039/JR9610002601**.

66 N. Y. Turova, V. A. Kozunov, A. I. Yanovskii, N. G. Bokii, Y. T. Struchkov and B. L. Tarnopol'skii, Physico-Chemical and Structural Investigation of Aluminium Isopropoxide, *J. Inorg. Nucl. Chem.*, 1979, **41**(1), 5–11, DOI: **10.1016/0022-1902(79)80384-X**.

67 D. Chiche, M. Digne, R. Revel, C. Chanéac and J.-P. Jolivet, Accurate Determination of Oxide Nanoparticle Size and Shape Based on X-Ray Powder Pattern Simulation: Application to Boehmite AlOOH, *J. Phys. Chem. C*, 2008, **112**(23), 8524–8533, DOI: **10.1021/jp710664h**.

68 R. T. Tettenhorst and C. E. Corbató, Comparison of Experimental and Calculated X-Ray Powder Diffraction Data for Boehmite, *Clays Clay Miner.*, 1988, **36**(2), 181–183, DOI: **10.1346/CCMN.1988.0360213**.

69 D. Staub, S. Meille, V. L. Corre, J. Chevalier and L. Rouleau, Revisiting the Side Crushing Test Using the Three-Point Bending Test for the Strength Measurement of Catalyst Supports, *Oil Gas Sci. Technol. – Rev. D'IFP Energ. Nouv.*, 2015, **70**(3), 475–486, DOI: **10.2516/ogst/2013214**.

70 J. Blanchard, F. Ribot, C. Sanchez, P.-V. Bellot and A. Trokiner, Structural Characterization of Titanium-Oxo-Polymers Synthesized in the Presence of Protons or Complexing Ligands as Inhibitors, *J. Non-Cryst. Solids*, 2000, **265**(1), 83–97, DOI: **10.1016/S0022-3093(99)00885-6**.

71 A. B. Stiles, *Catalyst Supports and Supported Catalysts: Theoretical and Applied Concepts*, Butterworths, Boston, 1987.

72 K. S. W. Sing, Reporting Physisorption Data for Gas/Solid Systems with Special Reference to the Determination of Surface Area and Porosity (Recommendations 1984), *Pure Appl. Chem.*, 1985, **57**(4), 603–619, DOI: **10.1351/pac198557040603**.

73 K. Okada, T. Nagashima, Y. Kameshima and A. Yasumori, Effect of Crystallite Size on the Thermal Phase Change and Porous Properties of Boehmite, *J. Colloid Interface Sci.*, 2002, **248**(1), 111–115, DOI: **10.1006/jcis.2001.8183**.

74 M. Milanović, Z. Obrenović, I. Stijepović and L. M. Nikolić, Nanocrystalline Boehmite Obtained at Room Temperature, *Ceram. Int.*, 2018, **44**(11), 12917–12920, DOI: **10.1016/j.ceramint.2018.04.103**.

75 A. Mohsenzadeh, A. Zamani and M. J. Taherzadeh, Bioethylene Production from Ethanol: A Review and Techno-Economical Evaluation, *ChemBioEng Rev.*, 2017, **4**(2), 75–91, DOI: **10.1002/cben.201600025**.

76 T. K. Phung, L. Proietti Hernández, A. Lagazzo and G. Busca, Dehydration of Ethanol over Zeolites, Silica Alumina and Alumina: Lewis Acidity, Brønsted Acidity and Confinement Effects, *Appl. Catal., A*, 2015, **493**, 77–89, DOI: **10.1016/j.apcata.2014.12.047**.

77 M. Zhang and Y. Yu, Dehydration of Ethanol to Ethylene, *Ind. Eng. Chem. Res.*, 2013, **52**(28), 9505–9514, DOI: **10.1021/ie401157c**.

78 D. Fan, D.-J. Dai and H.-S. Wu, Ethylene Formation by Catalytic Dehydration of Ethanol with Industrial Considerations, *Materials*, 2013, **6**(1), 101–115, DOI: **10.3390/ma6010101**.

79 C. Angelici, B. M. Weckhuysen and P. C. A. Bruijnincx, Chemocatalytic Conversion of Ethanol into Butadiene and Other Bulk Chemicals, *ChemSusChem*, 2013, **6**(9), 1595–1614, DOI: **10.1002/cssc.201300214**.

80 A. Styskalik, I. Kordoghli, C. Poleunis, A. Delcorte, Z. Moravec, L. Simonikova, V. Kanicky, C. Aprile, L. Fusaro and D. P. Debecker, Hybrid Mesoporous Aluminosilicate Catalysts Obtained by Non-Hydrolytic Sol–Gel for Ethanol Dehydration, *J. Mater. Chem. A*, 2020, **8**(44), 23526–23542, DOI: **10.1039/D0TA07016E**.

81 X. Zhang, R. Wang, X. Yang and F. Zhang, Comparison of Four Catalysts in the Catalytic Dehydration of Ethanol to Ethylene, *Microporous Mesoporous Mater.*, 2008, **116**(1), 210–215, DOI: **10.1016/j.micromeso.2008.04.004**.

82 T. K. Phung, A. Lagazzo, M. Á. Rivero Crespo, V. Sánchez Escribano and G. Busca, A Study of Commercial Transition Aluminas and of Their Catalytic Activity in the Dehydration of Ethanol, *J. Catal.*, 2014, **311**, 102–113, DOI: **10.1016/j.jcat.2013.11.010**.

83 J. H. Kwak, D. Mei, C. H. F. Peden, R. Rousseau and J. Szanyi, (100) Facets of γ-Al_2O_3: The Active Surfaces for Alcohol Dehydration Reactions, *Catal. Lett.*, 2011, **141**(5), 649–655, DOI: **10.1007/s10562-010-0496-8**.

84 A. Styskalik, I. Kordoghli, C. Poleunis, A. Delcorte, D. D. Dochain, Z. Moravec, J. Vida, T. Homola, C. Aprile, L. Fusaro, F. Devred and D. P. Debecker, Non-Hydrolytic Sol–Gel Route to a Family of Hybrid Mesoporous Aluminosilicate Ethanol Dehydration Catalysts, *J. Mater. Sci.*, 2021, **56**(25), 14001–14018, DOI: **10.1007/s10853-021-06166-9**.

85 A. G. Marquez, P. Horcajada, D. Grosso, G. Ferey, C. Serre, C. Sanchez and C. Boissiere, Green Scalable Aerosol Synthesis of Porous Metal–Organic Frameworks, *Chem. Commun.*, 2013, **49**(37), 3848–3850, DOI: **10.1039/C3CC39191D**.